Journal of Power Sources 506 (2021) 230242

Contents lists available at ScienceDirect

Journal of Power Sources

journal homepage: www.elsevier.com/locate/jpowsour

Influence of orientation on ageing of large-size pouch lithium-ion batteries during electric vehicle life

Zoran Milojevic [a,c], Pierrot S. Attidekou [a,c], Musbahu Muhammad [b], Mohamed Ahmeid [a,c], Simon Lambert [a,c], Prodip K. Das [a,c,*]

[a] School of Engineering, Newcastle University, Newcastle upon Tyne, NE1 7RU, UK
[b] School of Computing, Engineering & Digital Technologies, Teesside University, Middlesbrough, TS1 3BX, UK
[c] The Faraday Institution, Quad One, Harwell Science and Innovation Campus, Didcot, UK

HIGHLIGHTS

- Thermal behaviour of pristine Li-ion pouch cell is influenced by its orientation.
- Flat oriented module's batteries aged more uniformly compared to vertically oriented ones.
- Ageing non-uniformity over the battery surface can be detected by EIS.
- Avoiding different orientations in the battery pack can prolong battery life.

GRAPHICAL ABSTRACT

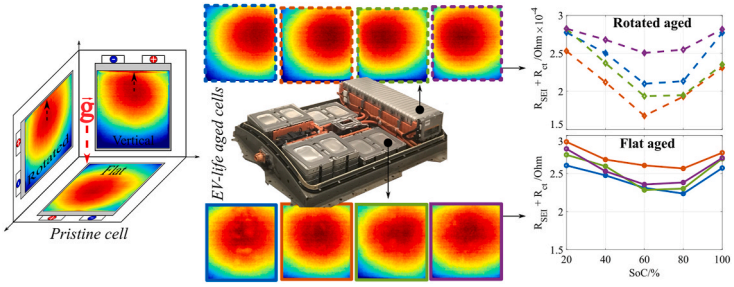

ARTICLE INFO

Keywords:
Lithium-ion batteries
Large-size pouch cell
Orientation influence
Ageing
Thermal imaging
Electrochemical impedance spectroscopy (EIS)

ABSTRACT

In the electric vehicle (EV) battery packs, large-size lithium-ion pouch batteries (LiBs) are mostly used and to miniaturise the battery pack's volume, some manufacturers put the LiBs in different orientations. It is well established that temperature gradients over large-size LiBs surface cause ageing non-uniformities, but the influence of the LiBs orientation on the ageing has to date received little attention. Here, we present an analysis of orientation influence on the large-size pouch LiB's ageing on eight batteries from two differently orientated modules from the dismantled first-generation Nissan Leaf retired battery pack. The influence of orientation is also analysed for brand-new second-generation Nissan Leaf battery which has almost the same geometry as batteries from the retired pack. By utilising infrared (IR) thermography and electrochemical impedance spectroscopy (EIS) techniques, the influence of orientation on the LiBs ageing non-uniformity is detected. Whilst temperature maps analysis shows different LiBs' thermal behaviour depends on their orientation, EIS measurements show that ageing non-uniformity can be identified by analysing the solid-electrolyte-interphase and charge-transfer resistances. Presented results show that different LiBs orientation in EV battery packs should be avoided because it can cause ageing non-uniformities over the battery surface and their second-life applications should be applied with caution.

* Corresponding author. School of Engineering, Newcastle University, Newcastle upon Tyne, NE1 7RU, UK.
E-mail address: prodip.das@newcastle.ac.uk (P.K. Das).

https://doi.org/10.1016/j.jpowsour.2021.230242
Received 19 March 2021; Received in revised form 22 June 2021; Accepted 2 July 2021
Available online 9 July 2021

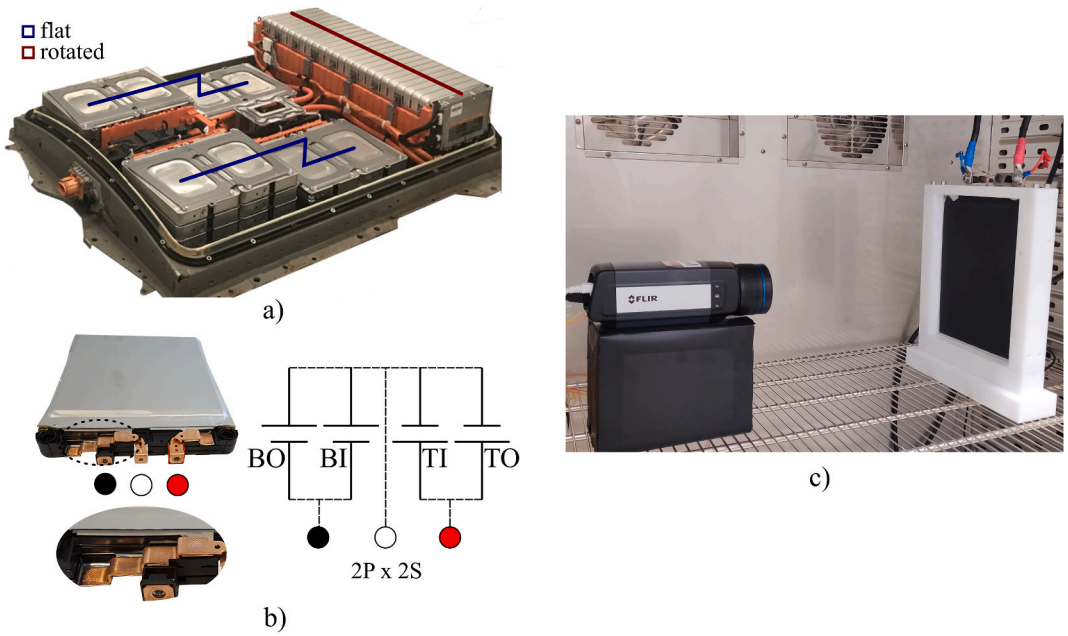

Fig. 1. a) Retired first-generation Nissan Leaf battery pack with different orientated modules, b) Battery cells connections in the module, c) Experimental setup during IR thermography imaging.

1. Introduction

Since the development of lithium-ion batteries (LiBs) in the 1970s, LiBs are ubiquitous in our daily life and present in almost all portable consumer goods. They have seen a significant amount of growth over the last decade in the areas of electric vehicles (EVs) and stationary storage applications due to their higher energy density and longer cycle life [1,2] and are now the cornerstone for moving towards zero-carbon futures and mitigating greenhouse gas emissions from the transportation sector [3]. LiBs in EVs finish their life with a significant amount of capacity left in them (~80% of the nominal capacity), which provides a promising avenue for reusing the spent EV-batteries in less demanding second-life applications, such as grid-scale energy storage and storage for intermittence energy sources (solar and wind electricity) [4,5]. However, reusing spent-EV batteries is not straightforward, whilst LiBs are complex electrochemical-thermal systems to understand and their ageing is even more complicated [6]. As batteries degrade over time and the capacity fading alone, cannot dictate whether a battery is suitable for safe use in the second-life application [7], a series of reliable characterisation tools or techniques are needed to ensure the maximum use of the spent EV-batteries and reduce system failures [8,9].

Ageing and degradation of LiBs over time is caused by cycling (application-based) and on storage [10] and leads to the battery capacity and power fade. The main factors associated with LiB degradation are charging/discharging rate (C-rate), operating temperature, lifetime, state of charge (SoC), cycling, etc. The influence of these factors on battery degradation mechanisms has already been widely studied [6,7,10–15]. When the size of the battery becomes large (large-size pouch LiB), it is important to consider dimensional effects, because variations of degradation factors such as local SoCs, operating temperatures and current densities should not be neglected [16–18]. During large-size LiB's life, these parameter variations can lead to non-uniform ageing over the battery surface.

One of the techniques that can be utilised in large-size pouch cell surface ageing analysis is infrared (IR) thermography, which is contactless, non-destructive and can measure temperature distribution with high spatial resolution. It is mostly used for validation of results obtained from electrochemical-thermal and electro-thermal coupled models on pristine LiBs [19–23], but this technique provides the possibility to identify ageing non-uniformities also. Analysis of miscellaneously aged cells (calendar aged, high current cycled and low current cycled) and the possibility of an ex-situ non-uniform cell ageing characterisation is highlighted [24]. Robinson et al. [25] utilised IR thermography to detect internal defects in aged LiBs. Methodologies based on IR thermography in non-uniformity ageing and "real" end of life detection in LiB's second-life application are presented in Ref. [7]. Electrochemical impedance spectroscopy (EIS) is also a non-destructive technique that has been used to characterize electrochemical processes including the LiBs. EIS literature on lithium-ion batteries may be represented by typical papers such as those by Zhuang et al. [26] and Barai et al. [27]. A variety of models have been developed for Li-ion battery characterization [28–30]. The electrical circuit models use equivalent circuits, based on RC networks, to describe the dynamic behaviour of the batteries [8,31,32]. The literature clearly shows that the equivalent circuit model (ECM) offers an excellent approach in terms of modelling the transient and steady-state performance of LiBs.

In EVs, batteries are packed in the modules which are then connected to form a battery pack. Factors such as pack design, configuration, cooling methods as well as cells/modules orientation in a pack are influencing the battery degradation. To our best knowledge, there are no studies available in the open literature on battery degradation due to cells/modules orientation in a pack. Thus, we have investigated the effect of cell orientation on non-uniform battery ageing. In the experimental section of this paper, tested batteries' specifications and experimental procedures are presented. The methodology section explains the influence of gravity on active material particle wetting dependent on the battery orientation. The results section covers the thermal behaviours of a differently-orientated brand-new battery and differently orientated EV-life aged batteries. The last part in the results section presents EIS results of EV-life aged batteries.

2. Experimental

2.1. Batteries specification

For analysis purposes in this study, eight batteries were disassembled from the end-of-life (EoL) first-generation Nissan Leaf battery pack modules (lithium manganese oxide (LMO) with lithium nickel oxide

Table 1
Specifications of the tested batteries.

	F_{BO}	F_{BI}	F_{TI}	F_{TO}	R_{BO}	R_{BI}	R_{TI}	R_{TO}	BN
Q/Ah	28.7	28.6	28.2	28.2	27.9	27.8	27.7	27.7	56.3
Q_{nom}/Ah	32.5								56.3
L × W × T/mm	290 × 216 × 7								290 × 216 × 8
SoH/%	88.3	88.0	86.8	86.8	85.9	85.5	85.2	85.2	100

(LNO) cathode and graphite anode) with different orientations. The battery pack consists of 48 modules (passive cooled) which are arranged in two side-stacks (modules flat orientated – 2 × 12 modules) and one rear-stack (rotated modules 1 × 24) as shown in Fig. 1a. In every module, there are 4 pouch cells connected in 2P x 2S arrangement. To establish connections by bus-bars between cells in the module, cells' tabs were cut, and depending on their position in the module, cells are marked as bottom outside (BO), bottom inside (BI), top inside (TO) and top outside (TO) as shown in Fig. 1b. Also, in this study, a brand-new second-generation Nissan Leaf battery cell (lithium manganese cobalt oxide (NMC 532) cathode and graphite anode) was utilised, as the production of the first-generation Nissan Leaf batteries is discontinued. It is worth noting that the geometry of a second-generation battery is almost the same as the first-generation battery (it is only 1 mm thicker). The specifications of tested batteries are displayed in Table 1, where batteries with flat and rotated orientation are marked with F_{pos} and R_{pos} respectively and a brand-new second-generation battery is marked as BN.

2.2. Temperature measurement procedure

Batteries are cycled using CC-CV (1.5C compared to the battery nominal capacity Q_{nom}) and battery temperature is measured by the thermal camera (FLIR A655 sc) within the environmental chamber (Binder GmbH) during the discharge cycle (4.2 V–2.7 V). The environmental chamber temperature was set to 25 °C and during thermography measurements, the chamber was switched off to enable cells unified cooling conditions. IR camera was calibrated within the range −40 to 150 °C by the manufacturer and imaging is done in 640 × 480 resolution. Camera thermal sensitivity is less than 30 mK and maximal error is ±2%. The battery surface was painted by Tetanal Camera Varnish Spray/Black paint, with a measured emissivity value of 0.96 to eliminate reflection. A customised battery holder made from POM-C acetal solid plastic material and aluminium plates was used to keep the battery stable during imaging and facilitate connection with the tabs (Fig. 1c). Batteries were set in required orientation in the holder 72 h before measurement.

2.3. EIS measurement procedure

For EIS measurements, the batteries are charged up to 4.2 V (i.e. 100% SoC) and after 1-h of rest, the EIS experiment is performed for 100% SoC then discharged to the subsequent appropriate voltage corresponding to 80, 60, 40 and 20% SoC where the EIS is also performed after 1-h of rest. The experimental condition of EIS is in potentiostatic mode with a perturbation voltage amplitude, Va = 5 mV RMS over a frequency range of 5 kHz–10 mHz, at six points per decade. The EIS measurements were conducted in an environmental simulation chamber set at 25 °C capable of maintaining a constant temperature over the range −40 to 180 °C. The EIS measurements were collected using Bio-Logic HCP-1005 potentiostat.

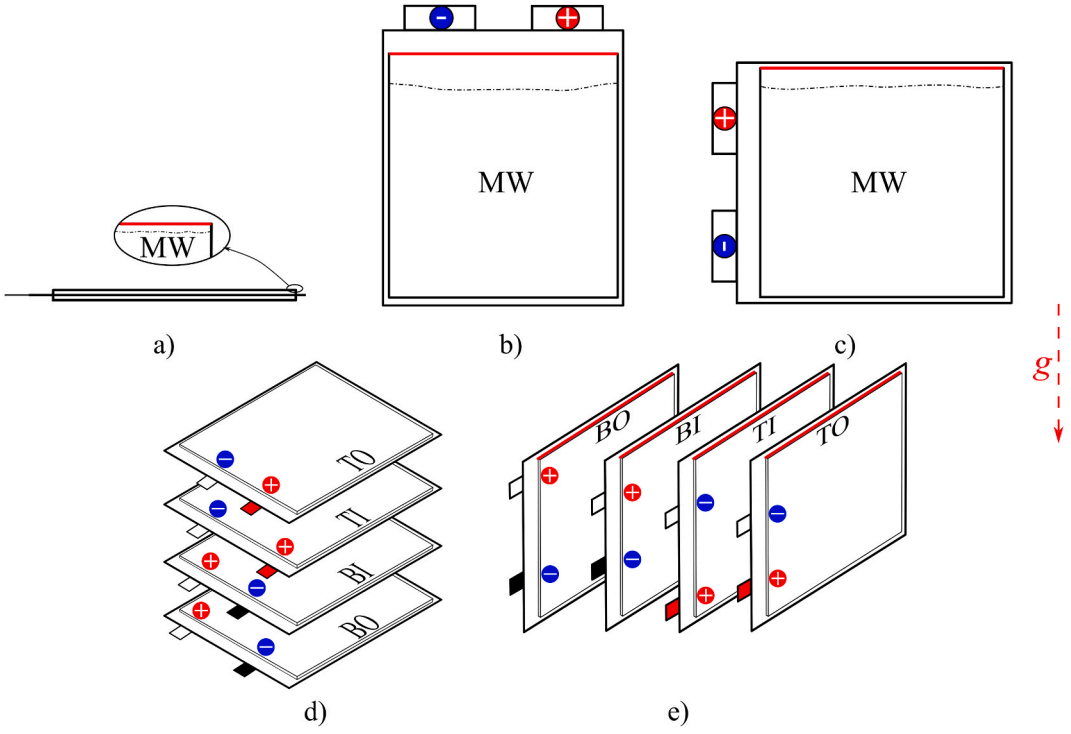

Fig. 2. Brand-new battery orientations during thermal imaging, a) flat, b) vertical and c) rotated and disassembled cells from two aged modules with d) flat and e) rotated orientation with tabs' signs and identification based on the position in the module.

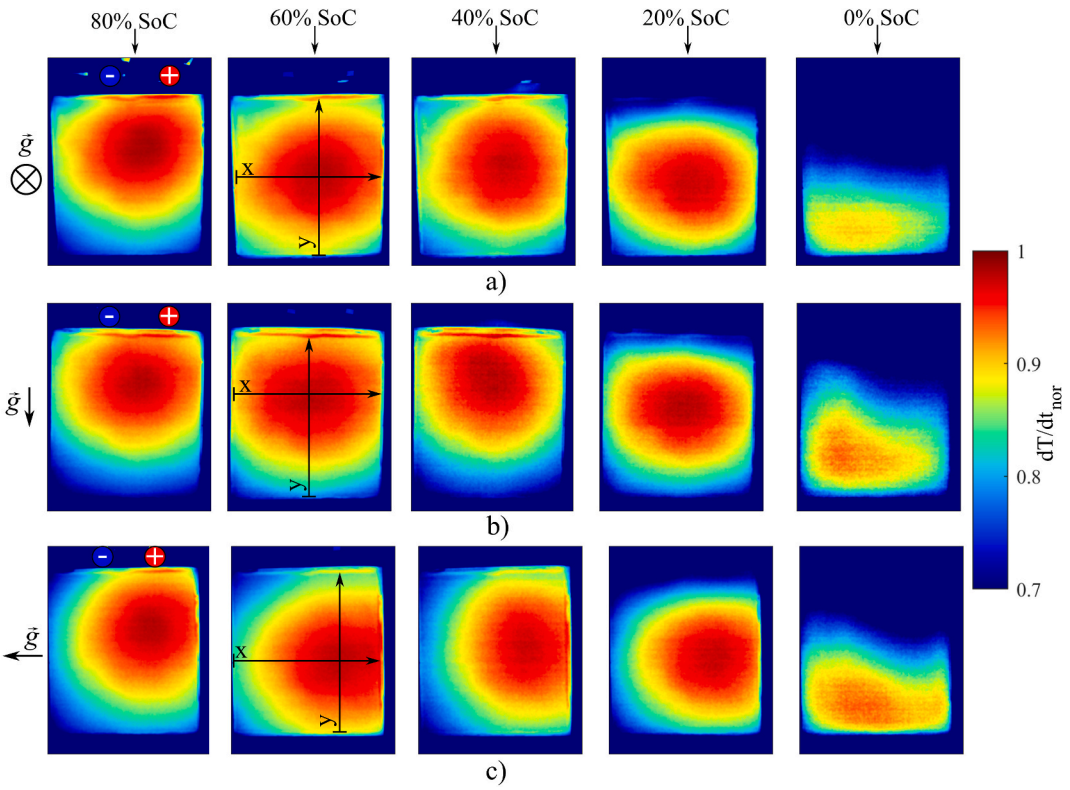

Fig. 3. Normalised rate of change of temperature (dT/dt_{nor}) maps of the brand-new battery measured at different orientations and SoCs, a) flat, b) vertical and c) rotated.

3. Methodology

The only material in the battery that can be influenced by different orientations and gravity is an electrolyte. Under the gravity at different battery orientations, particles from different battery areas can be more wetted (MW) in Fig. 2 with an electrolyte compared to the other ones. This can cause higher local resistances [33] and operational temperatures in the less wetted areas of the batteries compared to the MW areas. Furthermore, this can lead to inhomogeneous lithium concentrations and non-uniform current densities [34] which can lead to non-uniformly aged battery surface during the lifetime. In Fig. 2a, b and c, a brand-new battery in three different orientations, namely flat, vertical and rotated, are presented and the expected influence of the electrolyte position on the particle wetting is marked with a dash-dot line. The edge of the battery where higher resistance is expected caused by less wetted particles is marked with a red line for all three orientation cases. Similar to the brand-new battery, the orientation of batteries from the aged modules are presented in Fig. 2d (flat orientated) and Fig. 2e (rotated orientation during ageing) with edges where higher resistance is expected based on our hypothesis are marked with the red line. It is worth noting that the expected higher temperature for batteries (Fig. 2e) is closed to different tab's polarisations, which is dependent on the battery position in the module.

For qualitative thermal behaviour analysis (detection of a differently aged area on the cell surface), the temperature rate over time dT/dt maps is computed from temperature maps at every battery surface point. These maps can show more thermal non-uniformity compared to the measured temperature because local heat generation rates are more visible on them [7]. Stemming from the noise elimination of measured temperature, every surface point temperature over time is approximated with 5th order polynomial and dT/dt maps over the discharging time were generated. Also, in order to use the same scale for all thermal maps in this study, dT/dt values are normalised over the battery surface by dT/dt_{max} values. The normalised rate of change of temperature is stated as dT/dt_{nor} in the following sections. For indications of quantitative values obtained during the thermal imaging for aged cells, temperature standard deviation over the battery surface (σ_T) according to Ref. [7] and maximal temperature increase over the surface ($T_{\text{MAX-Rel}}$) are evaluated at specific SoCs.

EIS parameters were extracted using an equivalent circuit model (ECM) and the fitting of the data was performed using EC-Lab software (Zfit). A complex Non-Linear Least Squares (NLLS) based program was employed for the analysis by fitting the model parameters of the impedance spectrum to the measured spectrum. This is a recursive method where the NLLS starts with the initial model parameters provided by the user. These parameters are evaluated in the algorithm by an iterative method and replaced. If the fit is improved, the new parameter is accepted; in contrast, if the fit is not improved the previous parameter is retained and a different one is proposed and tested. This is repeated until the iteration converges to a criterion of acceptance evaluated by chi-square (χ^2) which is defined according to:

$$\chi^2 = \sum_{i=1}^{n} \frac{\left|Z_{meas}(i)^2 - Z_{model}\left(f_i, param\right)\right|^2}{\sigma_i^2} \quad (1)$$

where $Z_{meas}(i)$ is the measured impedance at the frequency f_i, Z_{model} (f_i, $param$) is the calculated impedance based on the chosen model, f_i is the frequency and σ_i is the standard deviation that can be equated to the weight of the impedance data points and this can be used to select the good circuit with a low level of noise. Besides, the relative error was estimated in terms of $\chi^2/(|Z|)$.

4. Results

In this section, first the results obtained from IR thermal imaging of a brand-new battery in different orientations are presented and then, IR thermal imaging and EIS results for EV-life aged batteries from the pack are shown.

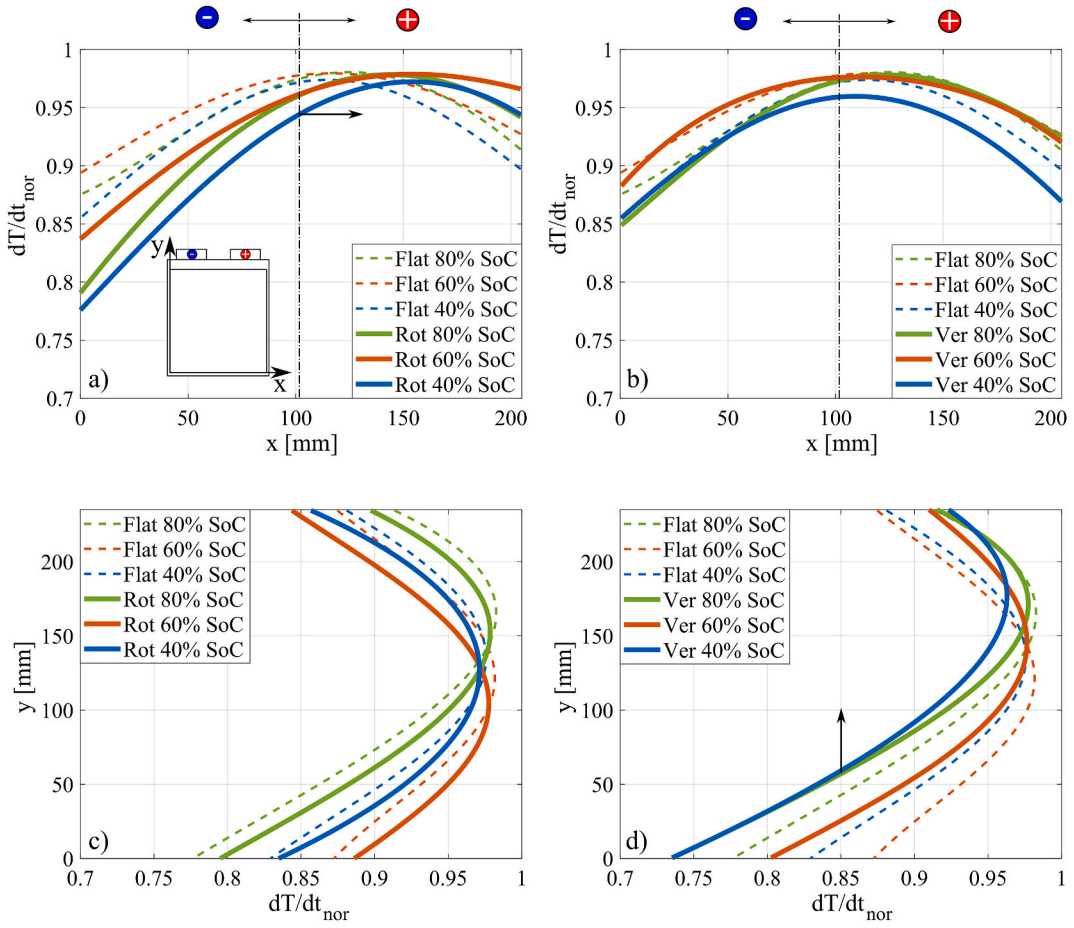

Fig. 4. Comparison graphs of dT/dt_{nor} maps cross-sections in *x*-direction flat-rotated (a) and flat-vertical (b) orientations, Comparison graphs of dT/dt_{nor} maps in *y*-direction cross sections for flat-rotated (c) and flat-vertical (d) orientations (arrows in parts (a) and (d) indicate the direction of hot-spot movement).

4.1. Thermal behaviour of the brand-new battery

Fig. 3 depicts the thermal behaviour of the brand-new battery in three different orientations, which are schematically shown in Fig. 2a–c. Here, the normalised rate of change of temperature (dT/dt_{nor}) maps are shown for various SoCs as indicated in the figure along with the direction of the gravity vector ($\vec{g}$). Comparing Fig. 3a (flat orientation) and Fig. 3b (vertical orientation) at high SoCs, it can be seen that the hot-spot position on the maps at the same SoCs for a vertically orientated battery is closer to the tabs. For the rotated battery (Fig. 3c), the hot-spot position is more towards the positive tab side. These maps are in good correlation with Fig. 2b and c where more heat is expected to be generated towards the marked battery edges. For a more detailed analysis of dT/dt_{nor} maps, cross-sections in *x* and *y* directions (marked in Fig. 3 for 60% SoC only) through thermal maps hot-spots are evaluated and presented in Fig. 4.

Fig. 4 shows the cross-section profiles of dT/dt_{nor} maps in the *x* and *y* directions for different battery orientations (flat-rotated and flat-vertical) for 80%, 60% and 40% SoCs. It can be seen that there is a significant difference in thermal behaviour in flat-rotated graphs (Fig. 4a) compared with flat-vertical graphs (Fig. 4b). For battery measured with rotated orientation highest dT/dt_{nor} values are shifted to the positive tab side compared to the flat-orientated measured battery where the graph is almost mirrored related to the battery symmetrical line (Fig. 4a). In Fig. 4b there is no significant difference between measurements done in flat and vertical orientations. Different behaviour can be seen for cross-section graphs evaluated in the *y*-direction (Fig. 4c and d). While there is no significant difference between flat and rotated orientation measurements graphs (Fig. 4c), a significant difference can be seen comparing flat and vertical measurements (Fig. 4d) where vertically orientated battery graphs are moved to the battery tabs' edge. Results presented in Fig. 4 further show that the hot-spot movement during battery IR thermal imaging at vertical and rotated orientations are in opposite directions according to the gravity vector direction during measurements (see Fig. 3b and c). These results clearly show that the influence of orientation has an impact on the battery thermal behaviour for the brand-new battery.

4.2. Thermal behaviour of EV-life aged batteries

Whilst the analysis of brand-new battery's thermal maps shown pure battery orientation influence (uniformly aged battery surface) on the battery thermal behaviour, EV-aged batteries will show ageing non-uniformity over the surface caused by battery different orientation during EV-life ageing. Comparing to the brand-new battery where IR thermal imaging is done at different orientations, for aged batteries, during measurements, all batteries were positioned at the same orientation (vertically oriented, similar to Fig. 2b). Also, batteries inside the pack were in flat and rotated positions (see Fig. 2d and e) only thermal maps cross-sections in the *x*-direction are presented. In Fig. 5, BO and BI positioned batteries thermal maps and hot-spot cross-sections in the *x* directions are shown. For flat positioned batteries during ageing can be seen that thermal maps cross-sections in the *x*-direction are almost symmetrical relative to battery symmetrical line (dashed lines in Fig. 5a and b right). Also, at 80% of SoC, there is no significant difference in flat and rotated aged batteries while at 60% and 40% of SoC there is a significant difference and rotated oriented batteries during the ageing show that higher dT/dt_{nor} values are more towards positive tab's side.

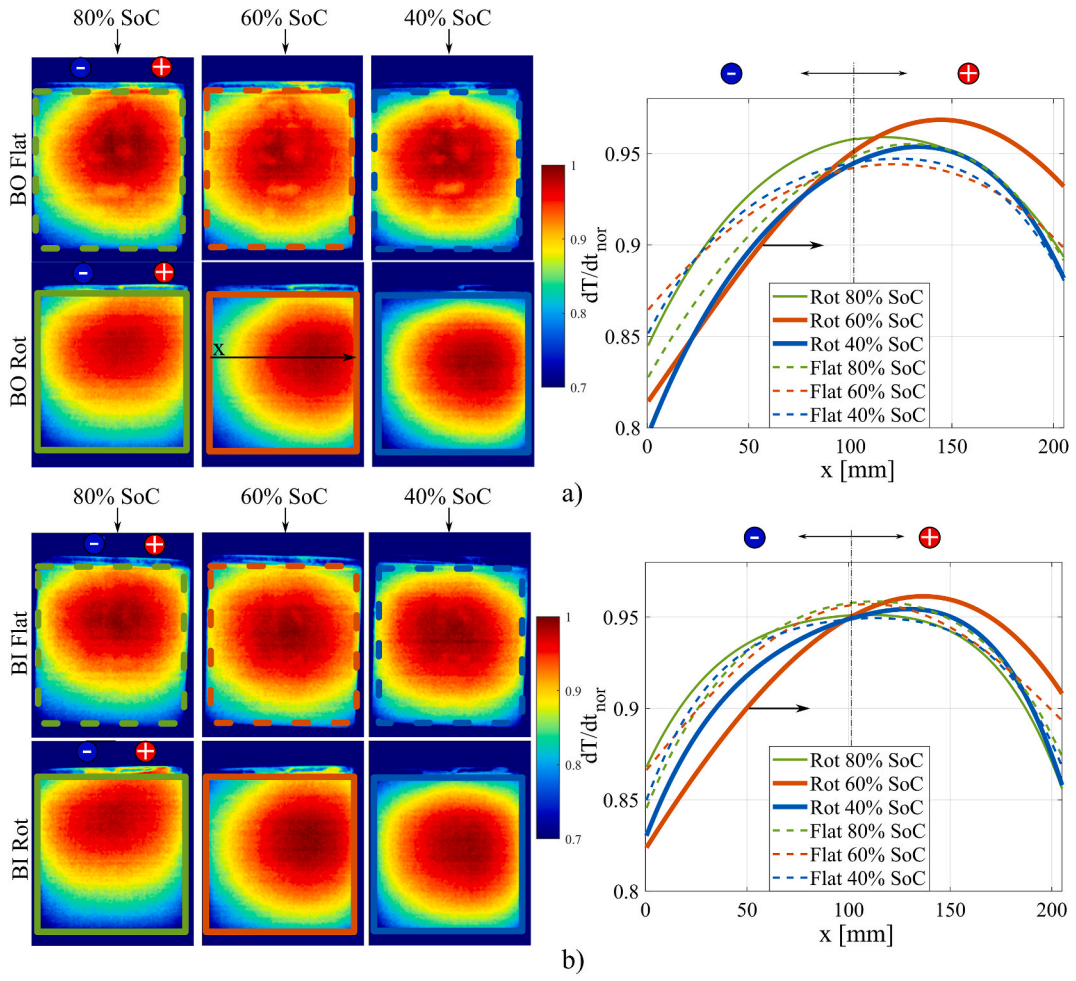

Fig. 5. a) Thermal maps of aged batteries with BO positions in the modules (left) and cross-sections through the hot spot in the *x*-direction (right); b) Thermal maps of aged batteries with BI positions in the modules (left) and cross-sections through the hot spot in the *x*-direction (right), where arrows in (a right) and (b right) indicate the direction of hot-spot movement).

Fig. 6 depicts TI and TO positioned aged batteries thermal maps and hot-spot cross-sections in the *x*-direction. It is observed for batteries aged in rotated and flat positions that hot-spot position at 80% SoC is on the positive tab's side and their behaviour is very similar. At 60% and 40% SoCs, different behaviour for rotated aged batteries (solid red and blue lines respectively) can be seen compared to the horizontally aged batteries (dashed red and blue lines respectively). Hot spot position is shifted to the negative tab's side for rotated aged batteries and this is more pronounced for TI compared to TO positioned battery during ageing.

In Table 2 temperature standard deviations (σ_T) and maximal temperature increase ($T_{MAX\text{-}Rel}$) over the battery surface at specific SoCs for aged batteries are presented. It is worth noting that both parameters are higher for rotated aged compared to flat aged batteries, and indicate more ageing of rotated ones, but can not indicate more aged surface areas as shown in Figs. 5 and 6.

4.3. EIS of EV-life aged batteries

In this section, the results of EIS analysis of aged batteries are presented. It is worth noting that the typical lithium-ion battery EIS spectrum is characterized by 4 different segments. The first segment can be observed below the real axis in the high-frequency region and is related to the connection of the lead wires. The second segment is represented by the crossing point of the EIS spectrum with the real axis. This point is attributed to the ohmic resistance (R_Ω) that encompassed the resistance of the electrolyte and the current collectors etc. The third segment is made of a semi-circle that can be observed in the medium frequency range. The semi-circle includes the solid-electrolyte interphase (SEI), the double-layer capacitance and the charge transfer resistance (R_{ct}). After the semi-circle in the lower frequency range segment 4, the diffusion tail can be observed. In this study, only the segment 2 and 3 will be considered and exploited.

Fig. 7 displays ECM used to fit the typical EIS spectra obtained at 100, 80, 60, 40 and 20% SoCs and their relative fitting curves for the position BI (flat and rotated batteries) respectively. The diagram of the ECM used to evaluate the data in this study is shown in Fig. 7a. The constant phase element (CPE) is employed and this is motivated by the surface roughness, the variation in thickness or composition, the non-uniform current distribution describing all together with the non-ideal behaviour of the system. The impedance of the CPE is defined as $Z(f_i) = [Q(J\omega_i)^n]^{-1}$ with $0 \leq n \leq 1$, where Q is the CPE and $\omega_i = 2\pi f_i$ is the angular frequency of the AC signal. When $n = 1$, the system behaves as a pure capacitor and when $n = 0$, it describes as a pure resistor. The ECM described herein, comprises a parallel branch of lead impedance (inductance (L) and resistance (R_L)) connected in series with the ohmic resistance (R_Ω). The series branch is then connected to another parallel branch one modelling the SEI layer (constant phase element (CPE_{SEI}) and SEI resistance (R_{SEI})), and the other represents the double-layer capacitance constant phase element (CPE_{DL}), charge transfer resistance (R_{ct}) and constant phase element (CPE_S) associated with the interfacial process at the double-layer. Finally, a diffusion element is

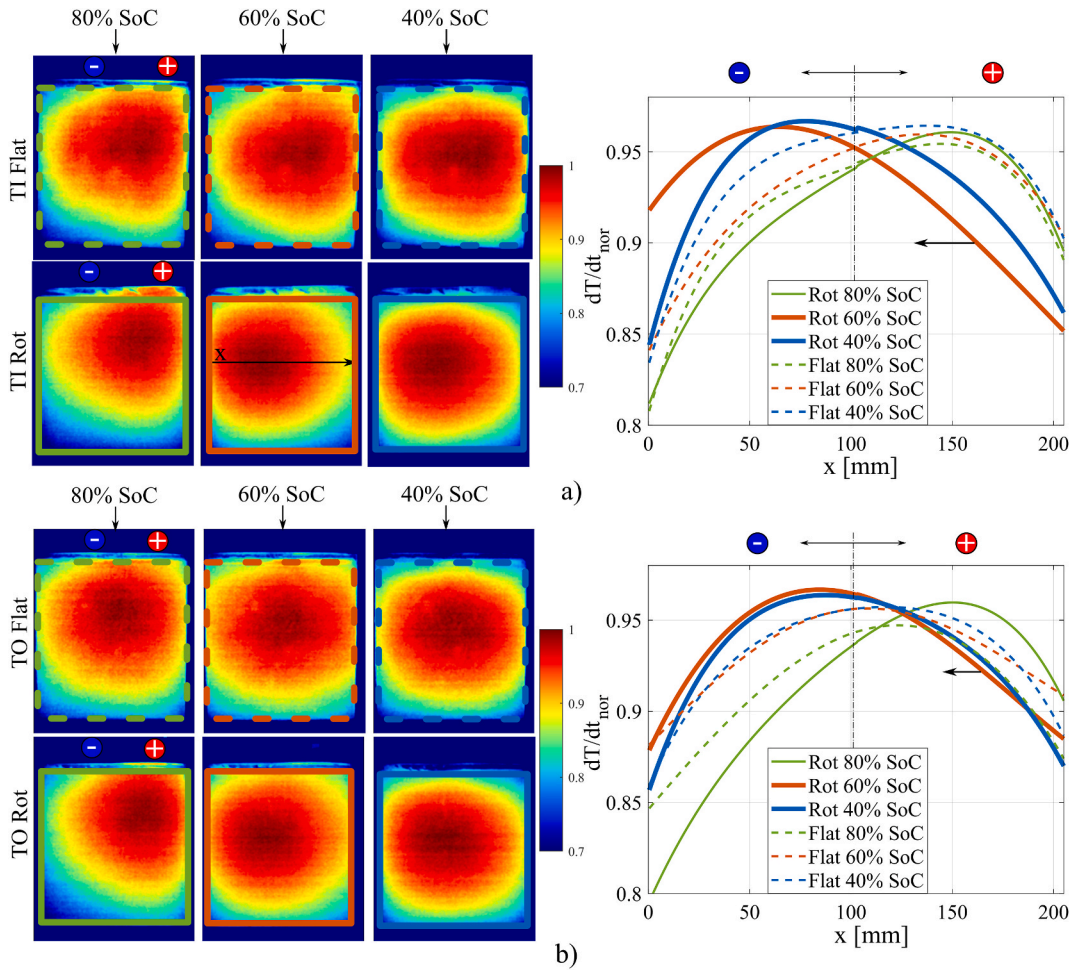

Fig. 6. a) Thermal maps of aged batteries with TI positions in the modules (left) and cross-sections through the hot spot in the x-direction (right); b) Thermal maps of aged batteries with TO positions in the modules (left) and cross-sections through the hot spot in the x-direction (right), where arrows in (a right) and (b right) indicate the direction of hot-spot movement).

Table 2
Temperature standard deviations (σ_T) and the maximal temperature increase ($T_{MAX\text{-}Rel}$) over the surface for aged batteries at specific SoCs.

	σ_T/°C			$T_{MAX\text{-}Rel}$/°C		
SoC/ %	80% SoC	60% SoC	40% SoC	80% SoC	60% SoC	40% SoC
F_{BO}	0.23	0.31	0.38	3.8	6.1	8.0
F_{BI}	0.22	0.31	0.37	3.9	6.1	8.0
F_{TI}	0.23	0.33	0.41	3.8	6.2	8.2
F_{TO}	0.24	0.33	0.41	3.8	6.3	8.3
R_{BO}	0.26	0.37	0.48	3.9	6.3	8.4
R_{BI}	0.26	0.37	0.45	3.9	6.5	8.5
R_{TI}	0.27	0.38	0.47	4.1	6.6	8.9
R_{TO}	0.27	0.38	0.45	4	6.6	8.9

connected in series with these branches as shown in Fig. 7a.

As can be seen from these figures (Fig. 7b–f), there is a noticeable difference between the impedance spectra collected on the flat and rotated batteries and this at all investigated SoCs. Firstly, the ohmic resistances of the flat battery are systematically lower compared to that of the rotated-battery and this is observed at all SoCs. Besides, the semi-circle of the flat batteries is systematically bigger compared to that of the rotated batteries and this is also observed at all aforementioned SoCs. These differences can be attributed to the orientation of the batteries during ageing. And this will be addressed in the discussion section.

Fig. 7b–f shows the typical Nyquist plots of the batteries with flat and rotated orientations at 20, 40, 60, 80 and 100% SoC collected at 25 °C and their relative fitting data so obtained. The fitting parameters are tabulated in Table 3 as well as the χ^2 and the relative error. As can be seen, from these Fig. 7b–f a good fit was obtained for the impedance data within $3.54 \times 10^{-9} \leq \chi^2 \leq 23.6 \times 10^{-9}$ and with $1.22 \times 10^{-3} \leq \chi^2/|Z| \leq 8.55 \times 10^{-3}$.

The parameters of interest obtained from the fitting data i.e. R_{SEI} and R_{ct} are added together and plotted as a function of SoCs in Fig. 8a–f. Similar shapes were observed for all the plots of the sum of the aforementioned resistances versus SoCs. As can be seen in Fig. 8a and b, the sum of resistances decreases from 100% SoC to a minimum around 80 or 60% SoC before increasing in the region of 40 to 20% SoCs. However, when comparing the sum resistance of the 4 cells from the differently orientated modules, the values of the cells in flat orientation (Fig. 8a) are in a narrower range compared to that of the rotated Fig. 8b. Fig. 8c–f shows the cells in the identical position but with different orientations two by two and it is clear that except for the cells in position top outside (TO), the resistances of the flat-cells are higher than that of the rotated cells and this will be explained in the discussion section.

5. Discussion

It is clear from the present results that for pristine large-size LiB, battery orientation has a significant influence on battery thermal behaviour. The position of the hot spot on the temperature derivative maps is closer to the battery edges which are opposite to the gravity

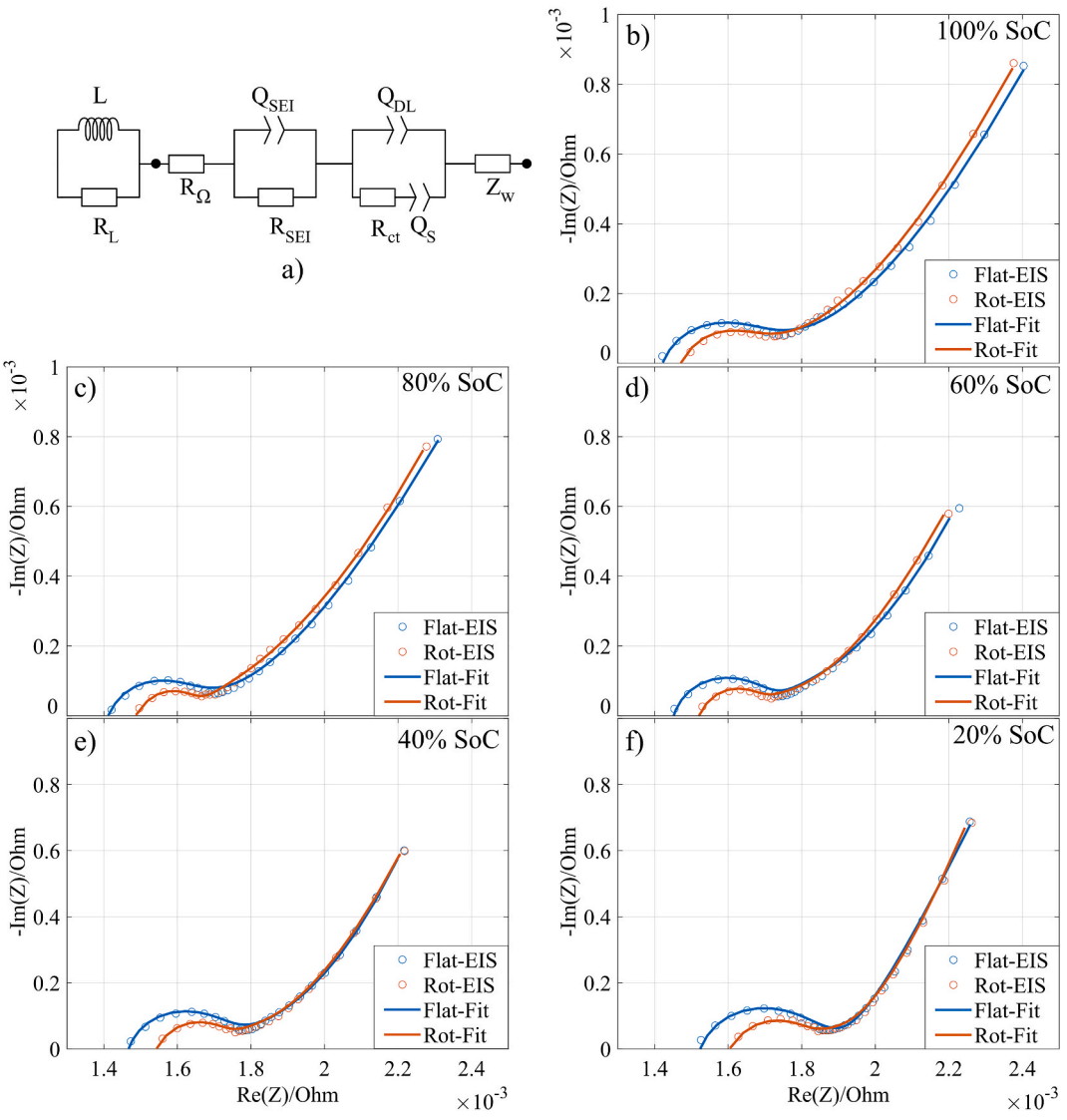

Fig. 7. ECM scheme for EIS data fitting (part a) and EIS and fitted data comparison for batteries with different orientations with the same positions (BI) in the modules at specific SoCs (parts b-f).

Table 3
Fitting parameters obtained from the EIS.

Parameter	Flat orientation					Rotated orientation				
SoCs/%	100	80	60	40	20	100	80	60	40	20
L/H ($\times 10^{-9}$)	32.3	32.3	30.4	28.3	35	82.6	62.3	71.4	83.0	95
R_L/Ohm ($\times 10^{-3}$)	10	10	10	12.6	10.5	10	10	20	12	10
R_Ω/Ohm ($\times 10^{-3}$)	1.37	1.35	1.42	1.43	1.47	1.41	1.43	1.45	1.48	1.52
R_{ct}/Ohm ($\times 10^{-4}$)	2.7	2.5	2.5	2.6	2.8	2.2	1.9	1.6	2.0	2.4
R_{SEI}/Ohm ($\times 10^{-5}$)	1.3	0.87	0.86	0.83	1.26	1.11	0.81	0.55	0.91	1.7
CPE_{DL}/Fs^{-n} ($\times 10^{-2}$)	2.18	2.38	2.39	2.39	2.36	2.89	3.62	3.56	3.57	3.33
CPE_{SEI}/Fs^{-n} ($\times 10^{-2}$)	1.96	1.93	2.61	2.77	3.16	1.82	1.83	2.74	2.74	3.49
CPE_S/Fs^{-n} ($\times 10^{-4}$)	2.87	2.55	2.12	2.23	1.48	2.86	2.56	2.38	1.97	1.64
n_{SEI}	0.75	0.75	0.82	0.81	0.77	0.8	0.87	0.92	0.86	0.8
n_{DL}	0.83	0.75	1	0.85	0.9	0.98	0.4	0.6	1	1
n_S	0.3	0.3	0.4	0.3	0.2	0.29	0.4	0.25	0.32	0.25
Rd/Ohm ($\times 10^{-5}$)	8.11	6.44	7.46	2.15	8.75	5.14	6.17	7.42	8.52	9.66
t/s	1.35	1.04	4.93	0.8	1.1	0.9	3.3	2	3	2
n	0.82	0.8	1	0.93	0.76	0.83	1	0.83	0.89	0.84
χ^2 ($\times 10^{-9}$)	7.84	11.32	23.6	22.41	6.52	3.54	5.68	5.9	4.5	4.55
$\chi^2/\|Z\|$($\times 10^{-3}$)	3.26	4.62	8.55	7.99	2.36	1.22	2.32	2.01	1.42	1.34

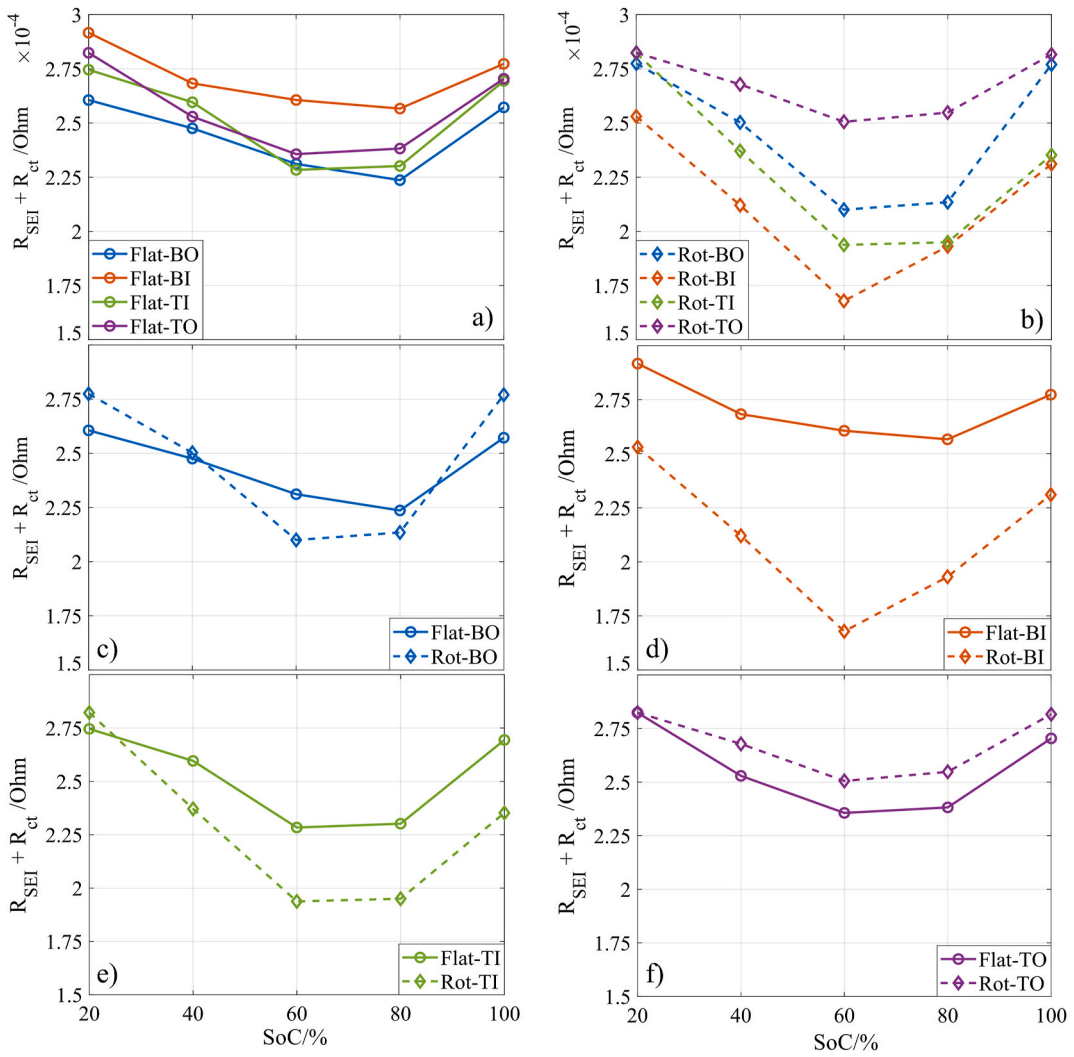

Fig. 8. The charge transfer and SEI layer resistances ($R_{SEI} + R_{ct}$) graphs for flat and rotated aged batteries (a and b respectively) and comparisons of differently orientated batteries with the same positions in the modules (c–f).

vector direction through a range of 80%–20% SoC. During EV-life, areas with less-wetted particles degrade faster, influenced by thermal gradients, local current densities, and higher local resistances opposite to the areas with more-wetted particles. The influence of such degradation mechanisms is shown on aged batteries from two modules orientated differently during lifetime disassembled from the EoL battery pack. While for brand-new batteries, different thermal behaviour is caused only by the difference in particles wetting during different battery orientations (uniformly aged surface) and shows a pure influence of the orientation on thermal behaviour, for aged batteries, different thermal behaviour is caused by batteries' surface ageing non-uniformities. Comparing the thermal behaviour of flat and rotated aged batteries (Figs. 5 and 6) with the brand-new battery at the same orientations and SoCs (Fig. 3a and c), thermal behaviour is very similar. It can be seen that hot-spot positions for horizontally orientated brand-new and aged batteries are in the middle of the battery, while for rotated orientated brand-new and aged batteries hot-spot is moved towards the edges marked by our hypothesis on Fig. 2c and e and are in good correlation.

Temperature derivative maps' hot-spot for rotated-aged batteries is closer to the battery edges which were opposite to the gravity vector direction during ageing but compared with the brand-new battery it is detectable through 60%–40% SoC range. Explanation of this lay in the fact that tabs are in mint condition for the brand-new battery compared to the aged batteries dismantled from the modules. This influences heat generation (caused by higher contact resistances from the tabs) and at the beginning of discharging heat from tabs is dominant over the heat generated in the battery active material [20–22].

Different parameters were extracted from the EIS refinements based on ECM presented. The ohmic resistance was excluded in our discussion because of batteries' tabs conditions. For the analysis of ageing non-uniformity of the battery surface, only charge transfer and SEI layer resistances (R_{SEI} and R_{ct}) are considered. During the EV-life the amount of liquid electrolyte becomes scarce due to ageing mechanisms and the charge transfer and SEI layer resistances are affected by the particle wettability and hence the surface. Based on the battery orientation and taking into account the effect of gravity, the batteries in the rotated orientation (except the cell from the top outside (TO) position) present a wider range of resistances compared to flat-orientated batteries, which can be linked to their higher ageing non-uniformity over the surface. Battery position in the module also influences battery ageing. For the BI and TI batteries (middle of the module), this behaviour is more pronounced, because there was more temperature influence on them during their lifetime. For the battery with TO position from the rotated orientation, thermal and EIS results show that ageing is more uniform compared to the other three batteries. The heat from the positive tab (Al) is higher compared to the negative tab (Cu) caused by lower Al electrical conductivity, and the positive tab position of TO battery is opposite to the battery edge where more ageing is expected caused by orientation

influence. That fact affected more uniform ageing compared to batteries positioned in the middle of the module and battery from the bottom outside (BO) position.

6. Conclusions

In this study, the influences of orientation on large-size pouch LiBs ageing have been investigated by IR thermography and EIS techniques. It is found that brand-new battery orientation influence due to gravity has a significant impact on the battery thermal behaviour. To understand how orientation influences battery ageing, eight cells from two differently orientated modules from the EoL EV battery pack were investigated. Results of IR thermography measurements analysis on retired pouch LiBs with different orientations show a different level of ageing non-uniformity over the battery surface. This is more pronounced for the battery aged in the rotated compared to the flat orientation inside the battery-pack. Moreover, EIS has shown a different range in resistances (charge transfer and SEI layer resistances) over SoCs and this has been attributed to non-uniformly aged surface. Moreover, based on the capacity and hence SoH, it is clear that cells aged in flat orientation retained higher capacity compared to the cells aged in rotated orientation. Further directions of this investigation will be focused on the material characterisation of differently orientated aged batteries to show a different material ageing state in surface areas detected by the proposed methodology. Also, orientation influence on the ageing will be investigated on the batteries from battery packs with an active cooling system. Based on the results presented, we conclude that different LiBs orientations should be avoided to maintain uniform ageing over the whole battery pack. Different battery orientations inside the pack can cause ageing non-uniformities over the battery surface and their second-life applications should be applied with caution. Also, for the second-life application, extensive care should be taken to assemble batteries with the same orientation during ageing.

CRediT authorship contribution statement

Zoran Milojevic: Conceptualization, Methodology, Investigation, Validation, Data curation, Formal analysis, Writing – original draft, Writing – review & editing. **Pierrot S. Attidekou:** Conceptualization, Methodology, Investigation, Validation, Data curation, Formal analysis, Writing – original draft, Writing – review & editing. **Musbahu Muhammad:** Validation, Investigation, Writing – review & editing. **Mohamed Ahmeid:** Data curation, Investigation, Validation. **Simon Lambert:** Funding acquisition, Project administration. **Prodip K. Das:** Conceptualization, Formal analysis, Supervision, Funding acquisition, Writing – review & editing.

Declaration of competing interest

The authors declare that they have no known competing financial interests or personal relationships that could have appeared to influence the work reported in this paper.

Acknowledgements

This work was part of ReLiB project (https://relib.org.uk/) and was supported by the Faraday Institution [grant number FIRG005].

References

[1] J.B. Goodenough, K.-S. Park, The Li-ion rechargeable battery: a perspective, J. Am. Chem. Soc. 135 (2013) 1167–1176, https://doi.org/10.1021/ja3091438.
[2] L. Lu, X. Han, J. Li, J. Hua, M. Ouyang, A review on the key issues for lithium-ion battery management in electric vehicles, J. Power Sources 226 (2013) 272–288, https://doi.org/10.1016/j.jpowsour.2012.10.060.
[3] G. Harper, R. Sommerville, E. Kendrick, L. Driscoll, P. Slater, R. Stolkin, A. Walton, P. Christensen, O. Heidrich, S. Lambert, Recycling lithium-ion batteries from electric vehicles, Nature 575 (2019) 75–86, https://doi.org/10.1038/s41586-019-1682-5.
[4] L.C. Casals, B.A. García, C. Canal, Second life batteries lifespan: rest of useful life and environmental analysis, J. Environ. Manag. 232 (2019) 354–363, https://doi.org/10.1016/j.jenvman.2018.11.046.
[5] S. Tong, T. Fung, M.P. Klein, D.A. Weisbach, J.W. Park, Demonstration of reusing electric vehicle battery for solar energy storage and demand side management, J. Energy Storage 11 (2017) 200–210, https://doi.org/10.1016/j.est.2017.03.003.
[6] J. Vetter, P. Novák, M.R. Wagner, C. Veit, K.-C. Möller, J. Besenhard, M. Winter, M. Wohlfahrt-Mehrens, C. Vogler, A. Hammouche, Ageing mechanisms in lithium-ion batteries, J. Power Sources 147 (2005) 269–281, https://doi.org/10.1016/j.jpowsour.2005.01.006.
[7] P.S. Attidekou, Z. Milojevic, M. Muhammad, M. Ahmeid, S. Lambert, P.K. Das, Methodologies for large-size pouch lithium-ion batteries end-of-life gateway detection in the second-life application, J. Electrochem. Soc. 167 (2020) 160534, https://doi.org/10.1149/1945-7111/abd1f1.
[8] P.S. Attidekou, C. Wang, M. Armstrong, S.M. Lambert, P.A. Christensen, A new time constant approach to online capacity monitoring and lifetime prediction of lithium ion batteries for electric vehicles (EV), J. Electrochem. Soc. 164 (2017) A1792, https://doi.org/10.1149/2.0101709jes.
[9] M. Muhammad, M. Ahmeid, P. Attidekou, Z. Milojevic, S. Lambert, P. Das, in: 2019 IEEE 4th International Future Energy Electronics Conference (IFEEC), IEEE, 2019, pp. 1–5, https://doi.org/10.1109/IFEEC47410.2019.9015015.
[10] M. Broussely, P. Biensan, F. Bonhomme, P. Blanchard, S. Herreyre, K. Nechev, R. Staniewicz, Main aging mechanisms in Li ion batteries, J. Power Sources 146 (2005) 90–96, https://doi.org/10.1016/j.jpowsour.2005.03.172.
[11] A. Barré, B. Deguilhem, S. Grolleau, M. Gérard, F. Suard, D. Riu, A review on lithium-ion battery ageing mechanisms and estimations for automotive applications, J. Power Sources 241 (2013) 680–689, https://doi.org/10.1016/j.jpowsour.2013.05.040.
[12] F. Leng, C.M. Tan, M. Pecht, Effect of temperature on the aging rate of Li ion battery operating above room temperature, Sci. Rep. 5 (2015) 1–12, https://doi.org/10.1038/srep12967.
[13] C.R. Birkl, M.R. Roberts, E. McTurk, P.G. Bruce, D.A. Howey, Degradation diagnostics for lithium ion cells, J. Power Sources 341 (2017) 373–386, https://doi.org/10.1016/j.jpowsour.2016.12.011.
[14] Y. Gao, J. Jiang, C. Zhang, W. Zhang, Y. Jiang, Aging mechanisms under different state-of-charge ranges and the multi-indicators system of state-of-health for lithium-ion battery with Li (NiMnCo) O2 cathode, J. Power Sources 400 (2018) 641–651, https://doi.org/10.1016/j.jpowsour.2018.07.018.
[15] S. Atalay, M. Sheikh, A. Mariani, Y. Merla, E. Bower, W.D. Widanage, Theory of battery ageing in a lithium-ion battery: capacity fade, nonlinear ageing and lifetime prediction, J. Power Sources 478 (2020) 229026, https://doi.org/10.1016/j.jpowsour.2020.229026.
[16] G.-H. Kim, K. Smith, K.-J. Lee, S. Santhanagopalan, A. Pesaran, Multi-domain modeling of lithium-ion batteries encompassing multi-physics in varied length scales, J. Electrochem. Soc. 158 (2011) A955–A969, https://doi.org/10.1149/1.3597614.
[17] S. Jung, D. Kang, Multi-dimensional modeling of large-scale lithium-ion batteries, J. Power Sources 248 (2014) 498–509, https://doi.org/10.1016/j.jpowsour.2013.09.103.
[18] C. Veth, D. Dragicevic, R. Pfister, S. Arakkan, C. Merten, 3D electro-thermal model approach for the prediction of internal state values in large-format lithium ion cells and its validation, J. Electrochem. Soc. 161 (2014) A1943, https://doi.org/10.1149/2.1201412jes.
[19] U.S. Kim, C.B. Shin, C.-S. Kim, Modeling for the scale-up of a lithium-ion polymer battery, J. Power Sources 189 (2009) 841–846, https://doi.org/10.1016/j.jpowsour.2008.10.019.
[20] J. Yi, U.S. Kim, C.B. Shin, T. Han, S. Park, Three-dimensional thermal modeling of a lithium-ion battery considering the combined effects of the electrical and thermal contact resistances between current collecting tab and lead wire, J. Electrochem. Soc. 160 (2013) A437–A443, https://doi.org/10.1149/2.039303jes.
[21] A. Rheinfeld, S. Kosch, S.V. Erhard, P.J. Osswald, B. Rieger, A. Jossen, Electro-thermal modeling of large format lithium-ion pouch cells: a cell temperature dependent linear polarization expression, J. Electrochem. Soc. 163 (2016) A3046–A3062, https://doi.org/10.1149/2.0701614jes.
[22] S. Goutam, A. Nikolian, J. Jaguemont, J. Smekens, N. Omar, P.V.D. Bossche, J. Van Mierlo, Three-dimensional electro-thermal model of Li-ion pouch cell: analysis and comparison of cell design factors and model assumptions, Appl. Therm. Eng. 126 (2017) 796–808, https://doi.org/10.1016/j.applthermaleng.2017.07.206.
[23] E. Hosseinzadeh, R. Genieser, D. Worwood, A. Barai, J. Marco, P. Jennings, A systematic approach for electrochemical-thermal modelling of a large format lithium-ion battery for electric vehicle application, J. Power Sources 382 (2018) 77–94, https://doi.org/10.1016/j.jpowsour.2018.02.027.
[24] C. Veth, D. Dragicevic, C. Merten, Thermal characterizations of a large-format lithium ion cell focused on high current discharges, J. Power Sources 267 (2014) 760–769, https://doi.org/10.1016/j.jpowsour.2014.05.139.
[25] J.B. Robinson, E. Engebretsen, D.P. Finegan, J. Darr, G. Hinds, P.R. Shearing, D. J. Brett, Detection of internal defects in lithium-ion batteries using lock-in thermography, ECS Electrochem. Lett. 4 (2015) A106, https://doi.org/10.1149/2.0071509eel.
[26] Q.-C. Zhuang, X.-Y. Qiu, S.-D. Xu, Y.-H. Qiang, S.-G. Sun, Diagnosis of electrochemical impedance spectroscopy in lithium-ion batteries, Lithium Ion Batteries—New Developments 8 (2012) 189–227, https://doi.org/10.5772/26749.
[27] A. Barai, K. Uddin, W. Widanage, A. McGordon, P. Jennings, A study of the influence of measurement timescale on internal resistance characterisation

methodologies for lithium-ion cells, Sci. Rep. 8 (2018) 1–13, https://doi.org/10.1038/s41598-017-18424-5.
[28] U. Westerhoff, K. Kurbach, F. Lienesch, M. Kurrat, Analysis of lithium-ion battery models based on electrochemical impedance spectroscopy, Energy Technol. 4 (2016) 1620–1630, https://doi.org/10.1002/ente.201600154.
[29] T. Osaka, T. Momma, D. Mukoyama, H. Nara, Proposal of novel equivalent circuit for electrochemical impedance analysis of commercially available lithium ion battery, J. Power Sources 205 (2012) 483–486, https://doi.org/10.1016/j.jpowsour.2012.01.070.
[30] D.D. Macdonald, Reflections on the history of electrochemical impedance spectroscopy, Electrochim. Acta 51 (2006) 1376–1388, https://doi.org/10.1016/j.electacta.2005.02.107.
[31] P.S. Attidekou, S. Lambert, M. Armstrong, J. Widmer, K. Scott, P.A. Christensen, A study of 40 Ah lithium ion batteries at zero percent state of charge as a function of temperature, J. Power Sources 269 (2014) 694–703, https://doi.org/10.1016/j.jpowsour.2014.06.064.
[32] Y. Troxler, B. Wu, M. Marinescu, V. Yufit, Y. Patel, A.J. Marquis, N.P. Brandon, G. J. Offer, The effect of thermal gradients on the performance of lithium-ion batteries, J. Power Sources 247 (2014) 1018–1025, https://doi.org/10.1016/j.jpowsour.2013.06.084.
[33] S.J. An, J. Li, C. Daniel, H.M. Meyer III, S.E. Trask, B.J. Polzin, D.L. Wood III, Electrolyte volume effects on electrochemical performance and solid electrolyte interphase in Si-Graphite/NMC lithium-ion pouch cells, ACS Appl. Mater. Interfaces 9 (2017) 18799–18808, https://doi.org/10.1021/acsami.7b03617.
[34] C. Sauter, R. Zahn, V. Wood, Understanding electrolyte infilling of lithium ion batteries, J. Electrochem. Soc. 167 (2020) 100546, https://doi.org/10.1149/1945-7111/ab9bfd.